A model-based kinematic guidance method for control of underactuated autonomous underwater vehicles

Loïck Degorre, Thor Fossen, Olivier Chocron, Emmanuel Delaleau

▶ **To cite this version:**

Loïck Degorre, Thor Fossen, Olivier Chocron, Emmanuel Delaleau. A model-based kinematic guidance method for control of underactuated autonomous underwater vehicles. Control Engineering Practice, 2024, 152, pp.106068. 10.1016/j.conengprac.2024.106068 . hal-04690659

HAL Id: hal-04690659

https://hal.univ-brest.fr/hal-04690659v1

Submitted on 30 Sep 2024

HAL is a multi-disciplinary open access archive for the deposit and dissemination of scientific research documents, whether they are published or not. The documents may come from teaching and research institutions in France or abroad, or from public or private research centers.

L'archive ouverte pluridisciplinaire **HAL**, est destinée au dépôt et à la diffusion de documents scientifiques de niveau recherche, publiés ou non, émanant des établissements d'enseignement et de recherche français ou étrangers, des laboratoires publics ou privés.

Preprint

A Model-Based Kinematic Guidance Method for Control of Underactuated Autonomous Underwater Vehicles

Loïck Degorre[a], Thor I. Fossen[b], Olivier Chocron[c], Emmanuel Delaleau[c,*]

[a] *ENSTA Bretagne, UMR 6285, LABSTICC-Robex, 29200 Brest, France*
[b] *Department of Engineering Cybernetics Norwegian University of Science and Technology, 7491 Trondheim, Norway*
[c] *ENI Brest, UMR CNRS 6027, IRDL, 29200 Brest, France*

Abstract

In this work, a novel guidance principle for underactuated autonomous underwater vehicles is introduced. This new method relies on the kinematic coupling between non-actuated and actuated degrees of freedom. It uses a newly introduced matrix called the *Handy Matrix* denoted $\mathcal{H}$. The method allows reassigning unused degrees of freedom of the task to useful non-actuated DOF. The algorithm and design rules leading to the construction of $\mathcal{H}$ are also provided. Two different solutions based on matrix $\mathcal{H}$ are compared on a standard seabed scanning task.

Keywords: AUVs, underactuated robots, model-based control, non-actuated DOF

1. Introduction

The emergence of new offshore underwater energy production technologies creates new applications for Autonomous Underwater Vehicles (AUVs). Notably, the need of frequent inspections and maintenance of these systems raises new dynamic maneuvering problems and requires enhanced mobility and agile vehicles. Also, the question of the cost and energy efficiency of these vehicles need to be addressed as they must remain both cheap and efficient to be a relevant solution for these applications.

Maneuvering problems are usually broken down into *path-following* and *trajectory-tracking* problems. In path following, the vehicle is controlled towards a desired path with no time constraint. Path-following control mainly focuses on the geometric part of the task, most often with open-loop dynamic control. Pioneering work on path following control of land vehicles can be found in (Samson, 1993; Micaelli and Samson, 1993). It was later on extended to marine vehicles in (Encarnacao and Pascoal, 2000) and (Lapierre et al., 2003; Lapierre and Soetanto, 2007). These works use a Serret-Frenet frame moving on the path and centered on the point of the path closest to the vehicle. A different approach can be found in (Breivik and Fossen, 2005) using a parallel transport frame (Bishop, 1975) parameterized by a path variable and a chosen propagation function. Additional, more recent works on path following methods can be found in the thorough review by (Hung et al., 2022) or in (Degorre et al., 2023) and the multiple

*Corresponding author
Email addresses: loick.degorre@ensta-bretagne.fr (Loïck Degorre), thor.fossen@ntnu.no (Thor I. Fossen), olivier.chocron@enib.fr (Olivier Chocron), emmanuel.delaleau@enib.fr (Emmanuel Delaleau)

references therein.

On the other hand, trajectory tracking includes both the geometric and dynamic parts of the task. In this case, the vehicle is aiming for a specific target on a path moving with prescribed dynamics. Examples of trajectory-tracking applications in the marine context can be found in (Alonge et al., 2001) or (Ashrafiuon and Muske, 2008).

Trajectory tracking has been chosen in this work as it allows for smoother and more accurate control of the vehicle all along the task than path following at the cost of higher computational complexity. Trajectory tracking is more suited for applications requiring high degrees of maneuverability.

This work is interested in the class of underwater vehicles considered *underactuated* either because they carry less thrusters than the number of degrees of freedom (DOF) solicited in the task or because their propulsive arrangement does not match with the task DOF requirements. In such a case, they are underactuated in the reduced configuration space of the task (Fossen, 2021) and are often referred to as *ill-actuated*. These vehicles represent a cheaper, more energy-efficient solution than the fully or over actuated ones but have reduced mobility that requires to be analyzed.

The goal of the guidance principle and controller introduced in this work is to make the best use of the actuated DOF of an underactuated vehicle to complete the trajectory-tracking task. Different solutions have been found to enhance the mobility of underactuated AUVs and use their capabilities at best. Most often, the control law of the vehicle can be designed to compensate for the lack of actuation over one DOF with another actuated one . This is notably the case with ill-actuated vehicles. Several examples of such compensating control laws can be found in the literature like in (Ashrafiuon and Muske, 2008; Elmokadem et al., 2019) where Sliding Mode Control is applied to an underactuated vehicle and where the sliding surfaces are designed to create this kind of behavior or in (Chen et al., 2023).

Guidance principles can also be used, outside of the control law, to create such compensating behaviors. The most notorious guidance method for marine vehicles is *Line-of-sight* (LOS) guidance (Breivik and Fossen, 2005). This method is inherited from traditional naval techniques and was originally designed for the control of underactuated surface ships actuated in surge and yaw but not in sway. The idea behind LOS guidance is to point the ship towards the destination and use sway motion to sail towards it. This method is most effective when rallying fixed, relatively far away waypoints of the horizontal plane (setpoint regulation) but has later been extended to path following and trajectory tracking tasks (Calvo et al., 2008; Borhaug et al., 2008; Caharija et al., 2016) both in 2D and 3D LOS algorithms are used to calculate new angle references for pitch and yaw (in 3D) or just for yaw (in 2D) relatively to the lateral (sway) and vertical (heave) errors. Then, any controller can be used to control the rotational DOFs of the vehicle towards the new reference values. (Fossen and Aguiar, 2024) discusses kinematic guidance laws rooted in the line-of-sight (LOS) principle. These methods are applicable to vehicles capable of controlling pitch and yaw angles. Our approach, in contrast, offers increased flexibility concerning underactuation.

The guidance principle introduced in this work follows the same idea as LOS Guidance but at the kinematic level. The idea is to use the kinematic couplings of the model to calculate new angular speed references based on linear speed commands on one or several other degree(s) of freedom. The controller makes use of a virtual reference point (VRP) on the vehicle called the *tracking point*. Several examples applying this technique to marine craft can be found in the literature (Berge et al., 1999; Alonge et al., 2001). Using a VRP has a natural stabilizing effect on the vehicle, just like pulling a shopping trolley is more stable than trying to push it. In this work, the VRP is taken at the bow of the craft under the water line, which enhances the roll and yaw stability of the vehicle.

The model manipulations leading to this new guidance principle are performed online in ongoing mission using a newly introduced *handy matrix* $\mathcal{H}$ and the algorithm provided to calculate it. This method can be seen as an extension of the work started in (Alonge et al., 2001) and deployed to fixed and vector thrusters AUVs in (Chocron and Delaleau, 2019b,a). Yet, these examples use asymmetrical

space reduction to introduce new compensation behaviors and are therefore hardly generalizable. Also, one of the advantages of this method is that it can creates several solutions to solve underactuation for a given system and task as will be seen in this example where either roll or yaw actuation can be used to compensate the non-actuated sway motion. Parallel work, dealing with 3D path following using a similar approach can be found in (Degorre et al., 2024) alongside a formal stability proof.

This paper is organized as follows. Section 2 gives a brief introduction to kinematic and dynamic models of the underactuated AUV. Then, Section 3 introduces the model-based feedback linearizing controller and the consequences of underactuation on the control inputs calculation. Finally, Section 4 introduces the main contribution of this work; the *handy matrix*, while Section 5 compares several simulation results using the proposed method.

2. Model of the Underactuated Autonomous Underwater Vehicle

This section briefly introduces the kinematic and the dynamic models of the underactuated AUV. Modeling of marine vehicles has been intensively studied throughout the last decades and the interested reader is referred to (Fossen, 2021; Antonelli, 2018) for more details about the establishment of the model. Also, note that the model parameters and the characteristics of the vehicle will be considered precisely known in the following work. Notably, the added mass and friction coefficients are considered precisely estimated. More details about these concepts can be found in (Lamb, 2005; Korotkin, 2009; Gartner et al., 2022).

The AUV chosen in this study is the *RSM*[1] Robot developed at IRDL-ENIB[2] and displayed in Figs. 1 and 2. The AUV has a cylindrical hull and is equipped with four fixed thrusters, two longitudinal at the stern and two vertical in the middle of the hull; see (Chocron et al., 2018) for the parameters corresponding to the *RSM* AUV model.

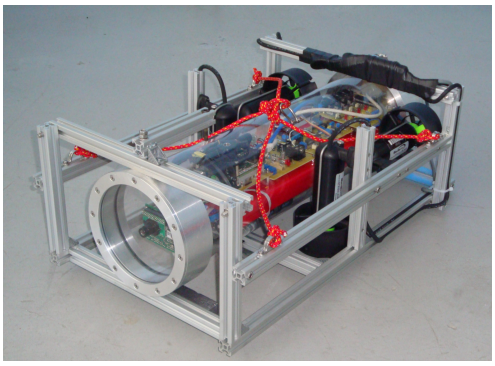

Figure 1: The *RSM* robot

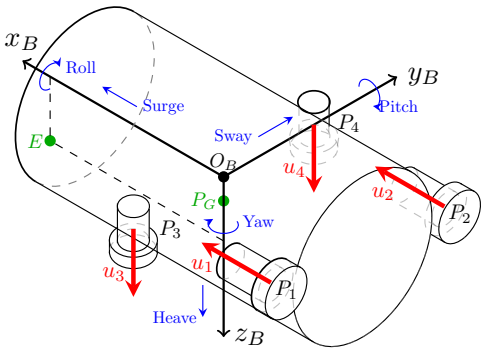

Figure 2: The propulsive configuration of the *RSM* robot. Points P_1–P_4 represent the four thrusters.

2.1. Framework

For convenience, two coordinate frames are defined: R_0 and R_B: $R_0(O, x_0, y_0, z_0)$ is the usual Earth-fixed North-East-Down (NED) reference frame and $R_B(O_B, x_B, y_B, z_B)$ is a mobile frame tied to the vehicle and centered at O_B. The two frames are depicted on Fig. 3. Note that point O_B could be chosen anywhere on the vehicle but is usually taken somewhere in the main planes of symmetry of the vehicle. In this example, O_B is chosen at the center of buoyancy in the center of the cylindrical hull and is different from the center of gravity P_G which is positioned slightly below for roll and pitch stability.

[1] *RSM*: *Robot sous marin* (in French), i.e. Submarine Robot.

[2] *Institut de recherche Dupuy de Lôme* (UMR-CNRS 6027), *École nationale d'ingénieurs de Brest*.

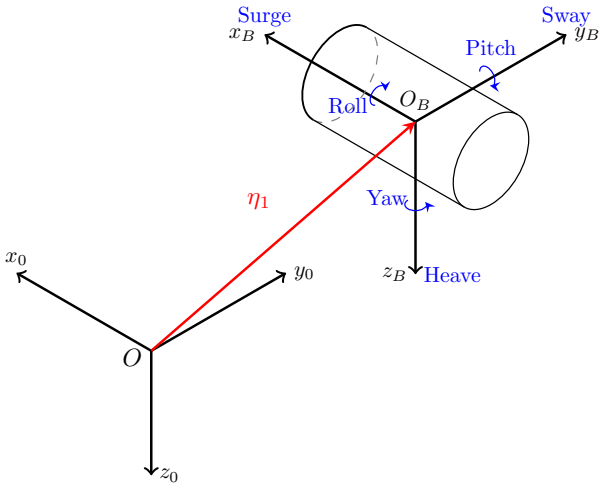

Figure 3: Earth-fixed $R_0(O, x_0, y_0, z_0)$ and body-fixed $R_B(O_B, x_B, y_B, z_B)$ frames. The x_B axis of the body-fixed frame is aligned with the cylinder axis.

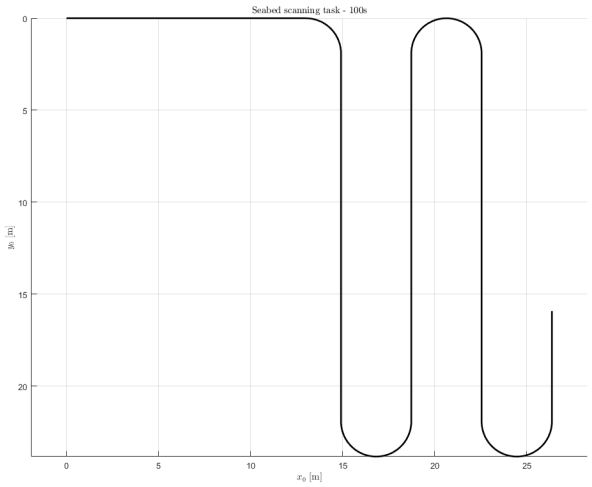

Figure 4: The seabed scanning trajectory (top view)

The task of the vehicle is called *seabed scanning* and is defined in R_0 as a succession of horizontal rails and turns at constant depth (see Fig. 4). The *tracking point* E (see Fig. 2) must follow the trajectory and the vehicle must stay tangential to the path at all times. The task thus requires four independent DOFs for the point E: surge, sway, heave and yaw.

2.2. Kinematic Model

The position and orientation of the vehicle in the inertial frame are denoted as $\eta = [\eta_1^\top, \eta_2^\top]^\top$ where $\eta_1 = [x, y, z]^\top$ is the position vector and $\eta_2 = [\phi, \theta, \psi]^\top$ is the orientation vector expressed with Euler angles in the roll-pitch-yaw convention. Additionally, the velocity of the AUV w.r.t. R_0 and expressed in R_B is denoted as $\nu = [\nu_1^\top, \nu_2^\top]^\top$ where $\nu_1 = [u, v, w]^\top$ is the linear velocity vector and $\nu_2 = [p, q, r]^\top$ is the angular velocity vector.

The kinematic model is given by:

$$\dot{\eta} = J(\eta_2)\nu \tag{1}$$

where $\dot{\eta}$ denotes the first time derivative of the vector η and $J(\eta_2)$ is defined in (Fossen, 2021) as:

$$J(\eta_2) = \begin{bmatrix} J_1(\eta_2) & 0 \\ 0 & J_2(\eta_2) \end{bmatrix} \tag{2a}$$

$$J_1(\eta_2) = R(x_0, \phi)R(y_0, \theta)R(z_0, \psi) \tag{2b}$$

$$J_2(\eta_2) = \begin{bmatrix} 1 & \sin(\phi)\tan(\theta) & \cos(\phi)\tan(\theta) \\ 0 & \cos(\phi) & -\sin(\phi) \\ 0 & \sin(\phi)/\cos(\theta) & \cos(\phi)/\cos(\theta) \end{bmatrix}, \ \theta \neq \pm\frac{\pi}{2} \tag{2c}$$

where $R(\chi, \lambda)$ is the rotation matrix of angle λ around axis χ.

Finally, the guidance method introduced in this work requires the definition of a *tracking point* E of coordinates $[\varepsilon_x, \varepsilon_y, \varepsilon_z]^\top$ in R_B that will be controlled towards the task. The *tracking point* or *virtual reference point* (VRP) can represent an effector, the focal point of a camera or any point of interest. The idea of using a VRP appears in the marine context in (Berge et al., 1999) and references therein. Using a tracking point at the bow of the vehicle increases the yaw stability, as if the vehicle were pulled by the VRP. Similar idea appears in (Alonge et al., 2001). In this work, let us consider E such that $\varepsilon_y = 0$, $\varepsilon_x > 0$ and $\varepsilon_z > 0$. The VRP is chosen at the bow, just under the (O_B, x_B, y_B) plane. Considering the

analogy of the shopping trolley introduced in (Berge et al., 1999), the advantage of the VRP appears intuitively. Choosing the tracking point at the bow of the vehicle passively enhances yaw stability and it is placed below the horizontal plane to create a sway-roll kinematic coupling.

The linear and angular velocities of point E in R_B are given in the vector ν_E defined as:

$$\nu_E = T\nu \tag{3}$$

where T is the transformation matrix given for E by:

$$T = \begin{bmatrix} \mathbb{I}_3 & S(E) \\ \mathbb{O}_3 & \mathbb{I}_3 \end{bmatrix} \tag{4}$$

where $\mathbb{I}_n$ is the identity matrix of size n, $\mathbb{O}_n$ is the zero matrix of size n, and S is the following skew-symmetrical matrix used to calculate a cross product:

$$S\left(\begin{bmatrix}\lambda_1\\ \lambda_2\\ \lambda_3\end{bmatrix}\right) = \begin{bmatrix} 0 & \lambda_3 & -\lambda_2 \\ -\lambda_3 & 0 & \lambda_1 \\ \lambda_2 & -\lambda_1 & 0 \end{bmatrix} \tag{5}$$

Here

$$S(E) = \begin{bmatrix} 0 & \varepsilon_z & 0 \\ -\varepsilon_z & 0 & \varepsilon_x \\ 0 & -\varepsilon_x & 0 \end{bmatrix} \tag{6}$$

2.3. Dynamic Model

The dynamic model of an underwater vehicle is (Fossen, 2021; Antonelli, 2018):

$$M\dot{\nu} + C(\nu)\nu + D(\nu)\nu + g(\eta) = \tau \tag{7}$$

where M is the matrix of mass and inertia, $C(\nu)$ is the matrix of Coriolis and centripetal terms, $D(\nu)$ is the damping matrix, $g(\eta)$ is the vector of gravitational and buoyancy forces and moments and τ is the vector of propulsive efforts. Note that the matrices in (7) are defined as:

$$M = M_a + M_b \text{ and } C = C_a + C_b$$

where M_b and C_b refer to the effects of the mass of the rigid body while M_a and C_a are due to hydrodynamic added mass (Fossen, 2021). The vehicle is considered of cylindrical shape and only the quadratic damping terms are collected in $D(\nu)\nu$. The vector $g(\eta)$ notably expresses the roll and pitch restoring moments due to the relative positions of O_B and P_G in R_B. The roll and pitch angles are naturally damped and converge to zero when not actively actuated. In the following analysis, and notably in the proof of Theorem 1, the roll and pitch motions can be considered zero-mean bounded motions when not actively controlled.

2.4. Propulsive Configuration of the Vehicle

The *RSM* Robot appears ill-actuated for the seabed scanning task presented in Section 2.1. Indeed, being equipped with four fixed independent, non-redundant thrusters, the *RSM* Robot has four actuated DOFs: surge, heave, roll and yaw, and two non-actuated DOFs: sway and pitch. Yet, the task in this example requires independent surge, sway, heave and yaw actuation (Chocron and Delaleau, 2019b). Therefore, compared to the task, the vehicle lacks sway actuation and has an additional roll motion useless for the task. Even if the vehicle has the proper number of actuated DOFs, the tracking problem is non-trivial because of the mismatch between the propulsive topology and the task requirements.

The propulsion forces generated by the four thrusters are:

$$\tau = \begin{bmatrix} X & 0 & Z & K & 0 & N \end{bmatrix}^\top \tag{8}$$

The vector τ is given by the four thruster forces and the *thruster configuration matrix* (TCM) B introduced in (Fossen and Johansen, 2006). From this it follows that:

$$\tau = Bu \tag{9}$$

where $u \in \mathbb{R}^4$ is the vector regrouping the thrust forces of each thrusters, one per line. Considering that the points of application of the four thrust forces are in the (O_B, x_B, y_B) plane, the TCM is given for this configuration as (Chocron and Delaleau, 2019a):

$$B = \begin{bmatrix} 1 & 1 & 0 & 0 \\ 0 & 0 & 0 & 0 \\ 0 & 0 & 1 & 1 \\ 0 & 0 & -R & R \\ 0 & 0 & 0 & 0 \\ R & -R & 0 & 0 \end{bmatrix} \tag{10}$$

where R is the radius of the AUV body-cylinder.

Note that the shape of τ introduced in (8) is directly induced by the shape of B. Indeed, in the absence of redundancies in the propulsive topology and with every thruster aligned with a frame axis, the non-actuated DOFs of τ (zero components) are direct consequences of the rows of zeros in B (rows 2 and 5). Thereby, regardless of the thrust values of u, the propulsive arrangement does not generate any sway force or pitch moment.

Also, in the underactuated case, B is not invertible by design, making thrust allocation non-trivial. In order to calculate the required thrusts for each thrusters of a given τ, the Moore-Penrose pseudo-inverse $B^\dagger$ can be used (Penrose, 1955). The pseudo-inverse gives a minimum error solution for u in (9). Another solution is to reduce the space of definition of the B matrix removing the rows corresponding to non-actuated DOF (rows 2 and 5 in the present example) (Vega et al., 2015). Because of the lines of zeros in B, these two solutions are equivalent but the first one is used:

$$u = B^\dagger \tau \tag{11}$$

with $B^\dagger$ the Moore-Penrose pseudo-inverse of B.

3. Controller

This section introduces the controller used in this work for the fully-actuated case first, and then for the underactuated case focusing on the consequences of underactuation. The control law is a model-based feedback linearizing controller, the AUV model is used in the controller to cancel the nonlinear terms and build a linear closed-loop system. This method has been extensively studied for the control of nonlinear systems with known models (Fossen, 2021; Martin and Whitcomb, 2018). Here, it is associated with PID-control but similar results could be obtained with Sliding Mode Control or any other control method (Yoerger and Slotine, 1985).

3.1. Feedback Linearization

Feedback linearization (Isidori, 1989; Nijmeijer and van der Schaft, 1990) is common practice when working with nonlinear systems such as the underwater vehicles. The control effort vector denoted τ_c will be based on the inverse dynamic model of the vehicle (7). In order to exactly linearize the model and create a simple linear closed-loop system, the matrices are evaluated at the current state of the vehicle. Other similar solutions use the desired state or an other state reference for linearization and some nonlinear terms can remain in the closed-loop system (Fjellstad and Fossen, 1994).

Here, the control vector is given in R_B by:

$$\tau_c = M\left(\dot{\nu}_c + K(\nu_c - \nu)\right) + C(\nu)\nu + D(\nu)\nu + g(\eta) \tag{12}$$

where ν_c is a velocity reference to be detailed below and K is a definite strictly positive gain matrix. The control law (12) clearly leads to the linear closed-loop system:

$$\dot{\nu} = \dot{\nu}_c + K(\nu_c - \nu) \tag{13}$$

Therefore, the control vector τ_c ensures convergence of the velocity of the vehicle towards the new speed reference ν_c. The speed reference itself is a control function designed to ensure convergence of the tracking point towards the desired trajectory, based on position/orientation errors. The reference is typically given by:

$$\nu_c = T^{-1}\tilde{\nu}_E \tag{14a}$$

$$\tilde{\nu}_E = J^{-1}\left[\dot{\eta}_d + K_p(\eta_d - \eta_E) + K_i \int_0^t (\eta_d - \eta_E)d\sigma\right] \tag{14b}$$

In the sequel one will denote e_x, e_y, and e_z the three position errors in R_0, i.e., the three first components of vector $\eta_d - \eta_E$. Equation (14) is a typical PI controller written in the inertial frame calculated with the error between the position and the orientation η_E of the tracking point E and the desired state η_d with K_p and K_i two strictly definite positive matrices. An anticipation term, $\dot{\eta}_d$, is used to complete the controller and make sure that when the position error is zero the reference speed is equal to the desired speed of the vehicle. Note that this control structure and notably the anticipation term require that the trajectory is at least $\mathcal{C}^2$. Using the kinematic model equations (1) and (3) the speed reference at point E in R_0 is transformed into the velocity control vector

ν_c expressed in the body-fixed frame R_B at the center of the vehicle O_B.

Again, this model-based structure leads to a virtual linear kinematic closed-loop system:

$$\dot{\eta}_E = \dot{\eta}_d + K_p(\eta_d - \eta_E) + K_i \int_0^t (\eta_d - \eta_E) d\sigma \quad (15)$$

Therefore, the speed reference ν_c can be seen as the virtual input of the kinematic controller ensuring convergence of the tracking point towards the desired trajectory. Roughly speaking, this control structure can be seen as a two-level cascaded controller where the outer stage is kinematic and generates the speed reference used in the dynamic inner stage. A block diagram of the two-stage controller can be seen on Fig. 5. Such structures are often used when working with nonlinear systems and are often referred to as *cascade control* or *hierarchical control* (Lévine and Rouchon, 1994). It is notably useful when the input and output of the system are defined in two rotating frames. The model-based cascade structure and the integral action of controller ensures good performance and natural robustness to (nearly) constant ocean currents (Degorre et al., 2024). Note also that the use of an integral term at the kinematic level provides robustness against the most common forms of disturbances experienced by marine craft. It notably allows rejecting constant forces created by ocean current or wind on the surface. The feedback linearizing controller (14) guarantees exponential convergence of the velocity tracking errors to zero. This is the key assumption for the Lypaunov stability analysis of the kinematic control law. In practice, there will be parametric and structural uncertainties. If the model is uncertain, it is recommended to replace the feedback linearizing control law with a sliding-mode controller (Yoerger and Slotine, 1985) or super-twisting adaptive sliding-mode controller (Shtessel et al., 2010). However, independent of the velocity controller, the kinematic controller is exponentially stable.

While the structure of the controller naturally provides robustness to external disturbances a switching term and sliding surface could be added in the inner loop to increase robustness.

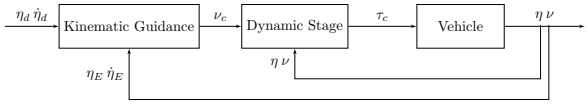

Figure 5: Block diagram of the two-stage controller in the general case

3.2. Consequences of Underactuation in the Control Law

In order to design a guidance principle compensating the non-actuated DOF of the vehicle, it is necessary to understand the consequences of the limitations of the propulsive topology on the controller. This section shows the problem raising from the application of the general controller introduced in Section 3.1 on the underactuated *RSM* robot. In order to perfectly follow the task, the vehicle should be able to generate independent surge, sway, heave and yaw efforts (Chocron and Delaleau, 2019b). Note that, even if the vehicle were able to perfectly track the yaw reference tangent to the path, sway actuation is mandatory, at least in the turns, to counteract dynamic and hydrodynamic effects. Yet, it cannot generate any sway force at point O_B. Consequently, regardless of the desired sway speed at the tracking point O_E, the control sway force is zero. At the kinematic level, one can consider that the corresponding control sway speed will always be zero as well. Obviously, same goes for the pitch of the vehicle but this DOF is not part of the task and is mechanically stabilized.

Considering the corrective velocity vector at the tracking point given in (14) $\tilde{\nu}_E = [\tilde{u}_E, \tilde{v}_E, \tilde{w}_E, \tilde{p}_E, \tilde{q}_E, \tilde{r}_E]^\top$, the kinematic part of the controller can be rewritten as:

$$u_c = \tilde{u}_E - \varepsilon_z \tilde{q}_E \quad (16a)$$
$$v_c = \tilde{v}_E + \varepsilon_z \tilde{p}_E - \varepsilon_x \tilde{r}_E \quad (16b)$$
$$w_c = \tilde{w}_E + \varepsilon_x \tilde{q}_E \quad (16c)$$
$$p_c = \tilde{p}_E \quad (16d)$$
$$q_c = \tilde{q}_E \quad (16e)$$
$$r_c = \tilde{r}_E \quad (16f)$$

But, because of the underactuated propulsive topology of the *RSM* robot, the sway and pitch control

speeds v_c and q_c at the center of the vehicle (O_b) are zero. Consequently, the kinematic stage becomes:

$$u_c = \tilde{u}_E - \varepsilon_z \tilde{q}_E \tag{17a}$$
$$0 = \tilde{v}_E + \varepsilon_z \tilde{p}_E - \varepsilon_x \tilde{r}_E \tag{17b}$$
$$w_c = \tilde{w}_E + \varepsilon_x \tilde{q}_E \tag{17c}$$
$$p_c = \tilde{p}_E \tag{17d}$$
$$0 = \tilde{q}_E \tag{17e}$$
$$r_c = \tilde{r}_E \tag{17f}$$

The main problem caused by underactuation in this case appears clearly in (17): because the sway corrective speed $\tilde{v}_E$ only appears in (17b) and has no control input in (O_b) it will be neglected in the calculation of the final control vector τ_c. This problem leads to faulty behaviors like parallel convergence. The vehicle would stabilize in parallel to the trajectory, canceling all errors but the lateral one. A simulation snapshot of this phenomena is provided on Fig. 6. On the snapshot, the vehicle is stabilized parallel to the trajectory, all errors are canceled but the lateral one which is neglected because of underactuation. In order to take the lateral error and thus the sway control speed at the tracking point into account, a kinematic guidance matrix is introduced in Section 4 and added to the controller.

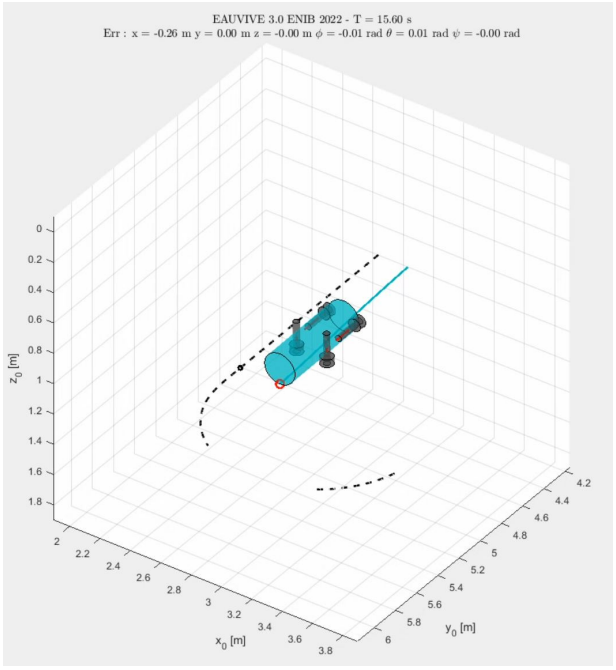

Figure 6: Simulation snapshot of parallel convergence due to neglecting $\tilde{v}_E$ in the controller — The vehicle is moving parallel to the trajectory (dashed) and the lateral error at point E (red dot) is neglected

4. Handy Matrix and Main Result

This section is the main contribution of this work. It introduces the kinematic guidance principle and the associated "Handy" matrix $\mathcal{H}$ used to compensate for the lack of sway actuation. This guidance method is based on well-known kinematic model manipulations integrated in the control law using the $\mathcal{H}$ matrix. As with LOS guidance and many other compensation mechanisms, a rotational DOF is used to cope for the lack of sway actuation and generate the required sway control velocity at the tracking point E.

4.1. Kinematic Guidance Principle

The idea of the kinematic guidance principle is to harness the kinematic couplings between the sway velocity at the tracking point E and the rotational velocities of the vehicle to compensate for the first with

one of the latter. In this case, considering the propulsive capabilities of the vehicle and the position of the tracking point only roll and yaw can be used to control sway. The kinematic couplings appear clearly in (17b). Hence, using (17d) and(17f), the two solutions are obtained:

$$1)\tilde{p}_c = -\frac{1}{\varepsilon_z}(\tilde{v}_E - \varepsilon_x \tilde{r}_E) \tag{18a}$$

$$2)\tilde{r}_c = \frac{1}{\varepsilon_x}(\tilde{v}_E + \varepsilon_z \tilde{p}_E) \tag{18b}$$

In the first case, the new roll reference velocity $\tilde{p}_c$ becomes a function of the sway control velocity at the tracking point, $\tilde{v}_E$, and therefore of the lateral tracking error while in the second case it is the yaw reference velocity $\tilde{r}_c$ that becomes a function of the sway controller $\tilde{v}_E$. Propagated to the dynamic part of the controller, these manipulations imply that the roll (respectively yaw) control moment is now a function of the sway control speed at the tracking point. Doing so means that the lateral error is no longer neglected and avoids parallel convergence. Actually, the behavior created by the $\mathcal{H}$ matrix is very close to the behavior created by other guidance methods. With LOS guidance for instance, the LOS reference angle (and therefore the corresponding control input) is a function of the transverse error which creates this behavior.

It also appears that the new reference velocities $\tilde{p}_c$ and $\tilde{r}_c$ are no longer functions of the corresponding control velocities, $\tilde{p}_E$ and $\tilde{r}_E$ respectively. Therefore, control over the DOF used for compensation is lost at the profit of the compensated one.

The new set of kinematic control equations is then given either by

$$\tilde{u}_c = \tilde{u}_E \tag{19a}$$
$$\tilde{v}_c = 0 \tag{19b}$$
$$\tilde{w}_c = \tilde{w}_E \tag{19c}$$
$$\tilde{p}_c = -\frac{1}{\varepsilon_z}(\tilde{v}_E - \varepsilon_x \tilde{r}_E) \tag{19d}$$
$$\tilde{q}_c = 0 \tag{19e}$$
$$\tilde{r}_c = \tilde{r}_E \tag{19f}$$

if roll is used for the sway compensation or by

$$\tilde{u}_c = \tilde{u}_E \tag{20a}$$
$$\tilde{v}_c = 0 \tag{20b}$$
$$\tilde{w}_c = \tilde{w}_E \tag{20c}$$
$$\tilde{p}_c = \tilde{p}_E \tag{20d}$$
$$\tilde{q}_c = 0 \tag{20e}$$
$$\tilde{r}_c = \frac{1}{\varepsilon_x}(\tilde{v}_E + \varepsilon_z \tilde{p}_E) \tag{20f}$$

if yaw is used for the sway compensation.

The compensation mechanism (19) or (20) has a double effect. It allows generating the exact sway speed calculated by the controller but, if the tracking point does not converge rapidly enough or if the lateral error is too large (typically greater than half of the hull length), it also progressively transfers the error from a non-actuated DOF towards an actuated one (provided there is one). Here, the error is transferred to heave if roll is used for compensation or to surge if yaw is used. Both heave and surge being actuated, the error will easily be canceled.

4.2. Introduction of the Handy Matrix $\mathcal{H}$

The idea behind the handy matrix $\mathcal{H}$ is to reproduce the manipulations of the kinematic model introduced in Section 4.1. To do so, a matrix is added in the calculation of the new reference speed $\tilde{\nu}_c$. The kinematic stage of the controller becomes:

$$\tilde{\nu}_c = \mathcal{H} T^{-1} \tilde{\nu}_E \tag{21}$$

where $\mathcal{H}$ is the new non diagonal matrix defined (see Section 4.3 for the calculation of $\mathcal{H}$) by $\mathcal{H}_p$ in the first case (where roll is used for compensation) and $\mathcal{H}_r$ in

the second case (where yaw is used):

$$\mathcal{H}_p = \begin{bmatrix} 1 & 0 & 0 & 0 & 0 & 0 \\ 0 & 0 & 0 & 0 & 0 & 0 \\ 0 & 0 & 1 & 0 & 0 & 0 \\ 0 & -1/\varepsilon_z & 0 & 1 & 0 & 0 \\ 0 & 0 & 0 & 0 & 0 & 0 \\ 0 & 0 & 0 & 0 & 0 & 1 \end{bmatrix}$$

$$\mathcal{H}_r = \begin{bmatrix} 1 & 0 & 0 & 0 & 0 & 0 \\ 0 & 0 & 0 & 0 & 0 & 0 \\ 0 & 0 & 1 & 0 & 0 & 0 \\ 0 & 0 & 0 & 1 & 0 & 0 \\ 0 & 0 & 0 & 0 & 0 & 0 \\ 0 & 1/\varepsilon_x & 0 & 0 & 0 & 1 \end{bmatrix} \quad (22)$$

Handy matrix $\mathcal{H}$ can be seen as a non-diagonal model-based gain matrix creating the new coupling between different DOF raised at the beginning of this work but this new control parameter has a fixed value imposed by the kinematic couplings of the system.

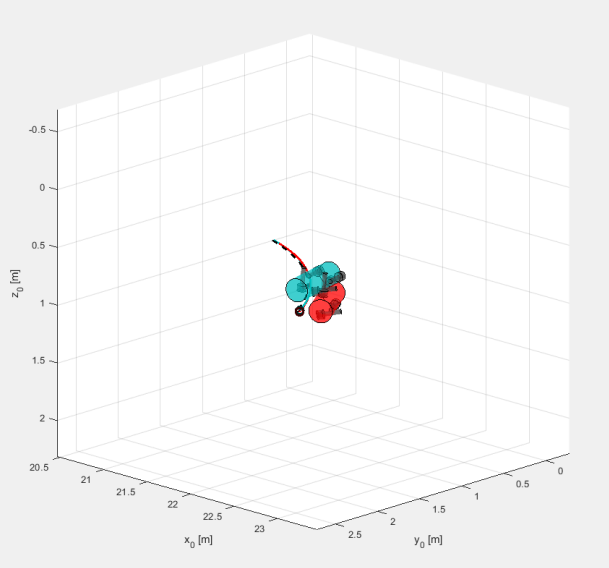

Figure 7: Simulation snapshot of the two guidance solutions $\mathcal{H}_p$ (Red) and $\mathcal{H}_r$ (Blue) — The blue vehicle stays upright but is not tangent to the trajectory in the turn, while the red one rolls to the side but stays tangent.

The two behaviors created by the matrices $\mathcal{H}_p$ and $\mathcal{H}_r$ are illustrated on Fig. 7. The difference between the two solutions appears clearly, with $\mathcal{H}_p$ (Red) the vehicle rolls to the side to generate the necessary sway speed in the turns but stays tangent to the trajectory whereas, with $\mathcal{H}_r$ (Blue), the vehicle overshoots the yaw angle to compensate for sway.

4.3. Calculation of the $\mathcal{H}$ Matrix

The computation of matrix $\mathcal{H}$ is detailed in this section. The algorithm designed to calculate the matrix uses two vectors defining the actuated DOF of the vehicle, h_{O_B}, and the DOF controlled at the tracking point E, h_E. Both vectors have a single column and one row per DOF where a "1" means actuated or controlled and a "0" means non-actuated or not controlled. The vectors are:

$$h_{O_B} = \begin{bmatrix} 1 \\ 0 \\ 1 \\ 1 \\ 0 \\ 1 \end{bmatrix} \text{ and } h_E^p = \begin{bmatrix} 1 \\ 1 \\ 1 \\ 0 \\ 0 \\ 1 \end{bmatrix} \text{ or } h_E^r = \begin{bmatrix} 1 \\ 1 \\ 1 \\ 1 \\ 0 \\ 0 \end{bmatrix} \quad (23)$$

The two possible choices h_E^p and h_E^r correspond to using either roll or yaw, respectively, to compensate for sway. In the first case, roll is used for compensation and yaw is controlled while in the second case it is the opposite.

In order for the algorithm to provide a viable $\mathcal{H}$ matrix and more widely for the compensation mechanism to work, three rules govern the choice of h_{O_B} and h_E:

1. The method can only be used if the tracking point E is different from the center of R_B, O_B and not located on the compensating rotation axis.
2. The method only allows compensation for linear velocities with angular velocities.
3. The method cannot be used to compensate a linear velocity with the angular velocity around the same axis.

The computation of $\mathcal{H}$ makes use of the skew-symmetrical cross-product matrix $S(\lambda)$. Notably, for point E of coordinates $\varepsilon = [\varepsilon_x, 0, \varepsilon_z]^\top$, it calculates Σ:

$$\Sigma = S([1/\varepsilon_x, 0, 1/\varepsilon_z]^\top) = \begin{bmatrix} 0 & -1/\varepsilon_z & 0 \\ 1/\varepsilon_z & 0 & -1/\varepsilon_x \\ 0 & 1/\varepsilon_x & 0 \end{bmatrix} \tag{24}$$

Algorithm 1 Calculation of the Handy matrix$\mathcal{H}$

$H \leftarrow \text{diag}(h_{O_B})$
$e \leftarrow [\varepsilon_x, \varepsilon_y, \varepsilon_z]^\top$
$\epsilon \leftarrow [0, 0, 0]^\top$
for $k = 1 : 3$
  if $e(k) \neq 0$
    $\epsilon(k) \leftarrow 1/e(k)$
$\Sigma \leftarrow S(\epsilon)$
for $i = 3 : 6$
  if $h_{O_B}(i) = 1$ **and** $h_E(i) = 0$
    for $j = 1 : 3$
      if $h_E(j) = 1$ **and** $h_{O_B}(j) = 0$ **and** $j \neq i - 3$
        $\mathcal{H}(i, j) \leftarrow \Sigma(i - 3, j)$

Outputs of this algorithm are given in (22). Overall, Algorithm 1 browses through the actuated rotational DOF of the vehicle, finds one rotation in h_{O_B} that has been disregarded in h_E and checks whether it is used to compensate a translation. When the rotation and translation are found, the appropriate ratio $1/\varepsilon_k$ (ε_k being the k^{th} coordinate of E in R_B) is selected in Σ and placed at the corresponding place in the bottom left corner of $\mathcal{H}$.

4.4. Main Result

In the sequel, the following assumptions are made:

A.1 The reference signal $\eta_d(t)$ is smooth and bounded for all $t \geqslant 0$.

A.2 The angular rate vector $\nu_2 = [p, q, r]^\top$ is measured and considered smooth and bounded for all $t \geqslant 0$.

Theorem 1. *The controller* (12)*, with* ν_c *defined as in* (21) *renders the origin* $e_x = e_y = e_z = 0$ *globally exponentially stable (GES) under Assumptions A.1–A.2 using either* $\mathcal{H}_p$ *or* $\mathcal{H}_r$ *of* (22)*.*

Proof. See Appendix Appendix A. □

5. Simulation Results

This section compares the two behaviors created by the two different compensation strategies corresponding to $\mathcal{H}_p$ and $\mathcal{H}_r$ and the newly introduced controller (12) with two standard controllers found in the literature: a LOS controller (Breivik and Fossen, 2005) and a Sliding Mode Controller (Elmokadem et al., 2016). These two control methods have been chosen for comparison with the proposed methods because they are very well established in the literature. LOS guidance is the most common and intuitive guidance principle, while SMC is a very well documented control method for non-linear systems in general. The results are provided by the Matlab *EAUVIVE* [3] (*IRDL-ENIB* [4]) numerical simulator. A numerical model of the *RSM* robot displayed on Fig. 1 is used in the following examples. Both tests are performed on the seabed scanning task introduced earlier. It is composed of a succession of horizontal rails at constant depth connected with circular turns. These rails must be followed by the tracking point E and the vehicle is constrained to stay tangent to the trajectory at all times. The parameters used in the simulations are shown in Tab. 1. The control parameters were first estimated with a pole placement technique and then empirically adjusted through trial and error.

Table 1: Simulation Parameters

Parameters	**Value**	**Added mass parameters**	**Value**
Mass	18.7 kg	$X_{\dot{u}}$	-1.88
Length	0.6 m	$Y_{\dot{v}}$	-18.8
Radius	0.2 m	$Z_{\dot{w}}$	-18.8
P_G	$[0, 0, 0.0125]^\top$	$K_{\dot{p}}$	0
O_E	$[0.2, 0, 0.2]^\top$	$M_{\dot{q}}$	-0.564
K	$8\mathbb{I}_6$	$N_{\dot{r}}$	-0.564
K_i	$2\mathbb{I}_6$	X_{uu}	-20.4
K_p	$8\mathbb{I}_6$	Y_{vv}	-156
Z_{ww}	-156	K_{pp}	-0.388
M_{qq}	-8.41	N_{rr}	-8.41

[3] EAUVIVE: Enhanced AUV In Virtuo Experiment.
[4] See Footnote 2.

5.1. Comparison of the two compensation strategies

Here, the two compensation strategies introduced earlier are compared on the seabed scanning task. In the first case, a roll speed is generated using $\mathcal{H}_p$ to compensate sway error at point E. In the second case, a yaw speed is generated using $\mathcal{H}_r$ to compensate the same error. The position and orientation errors of the two robots are given in Figs 8 and 9.

To keep the kinematic equivalence between the two solutions, the coordinates of point E were chosen as $\varepsilon_x = \varepsilon_z = 0.2$ m and $\varepsilon_y = 0$. Simulations show that the position of E is critical. Notably, if the offset (or lever) ε_z (respectively ε_x) gets too small, the performances are deteriorated.

As can be seen on Fig. 8, the performances of the two robots in terms of position tracking are comparable. The position errors are almost equal for both vehicles. The main difference between the two cases can be seen in the orientations on Fig. 9. Indeed, in the first case roll is disregarded in favor of sway and therefore roll disturbances can be observed on Fig. 9.(a). As well, a slightly larger pitch excursion is observed in the first case due to coupling effects in rotation when roll is different from 0. Nonetheless, neither roll nor pitch are part of the required DOF, such disturbances are therefore acceptable, especially as roll and pitch are mechanically stable in this system. When it comes to the yaw angle, performances are better in the first case using $\mathcal{H}_p$. Using $\mathcal{H}_r$ the yaw error rises up to 25° (twice as low in the first case). It is hardly acceptable considering that yaw is part of the requirements on this trajectory. This difference is easily understandable considering that tracking of the yaw angle is disregarded in the second case.

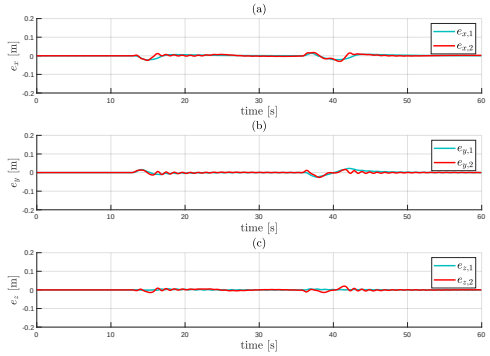

Figure 8: Comparison of the position errors in the inertial frame R_0 using the two guidance solutions $\mathcal{H}_p$ (Red) and $\mathcal{H}_r$ (Blue). Top: Error on the x_0 axis, Middle: Error on the y_0 axis, Bottom: Error on the z_0 axis

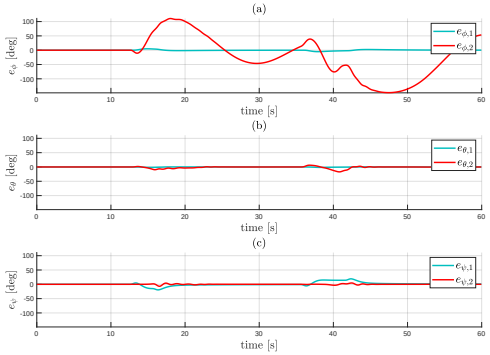

Figure 9: Comparison of the orientation errors using the two guidance solutions $\mathcal{H}_p$ (Red) and $\mathcal{H}_r$ (Blue). Top: Roll error, Middle: Pitch error, Bottom: Yaw error

5.2. Comparison with SMC and LOS

The new controller is compared with a Sliding Mode Controller (SMC) and a Line Of Sight guidance principle (LOS) of the literature. The SMC used for comparison is very similar to the controller proposed in (Elmokadem et al., 2016). The LOS controller is drawn from (Breivik and Fossen, 2005). In this example, the second compensation strategy $\mathcal{H}_r$ has been

chosen. Therefore, all three vehicles use yaw to compensate for the lack of sway. Note that the SMC includes this compensation behavior directly in the input calculation instead of relying on a guidance stage like the $\mathcal{H}_r$ matrix-based and the LOS controllers do.

Figs. 10 and 11 show that the new controller (Red line) demonstrates equally good trajectory tracking performances as the LOS (Blue) and SMC (Green) controllers. The three positions are almost perfectly tracked with the three controllers and the only remarkable difference appears on the yaw angle; The $\mathcal{H}_r$ matrix controller generates a smaller defection during the turns but the difference is not significant.

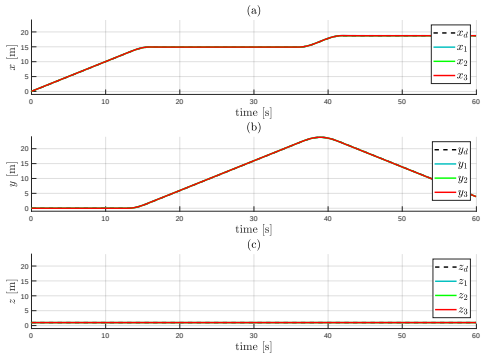

Figure 10: Comparison of the position of the vehicle using the three control methods. Blue line: LOS controller, Green line: SMC, Red line: Kinematic guidance principle using the $\mathcal{H}_r$ matrix. Top: Position on the x_0 axis, Middle: Position on the y_0 axis, Bottom: Position on the z_0 axis

6. Conclusion

A novel kinematic guidance principle for trajectory tracking of underactuated AUVs has been introduced in this work. It exploits the kinematic couplings between non actuated translations and actuated rotations to compensate the ill-actuation of the AUV. The guidance level of the controller calculates rotational reference velocities out of linear corrective velocities which are then used to calculate control forces

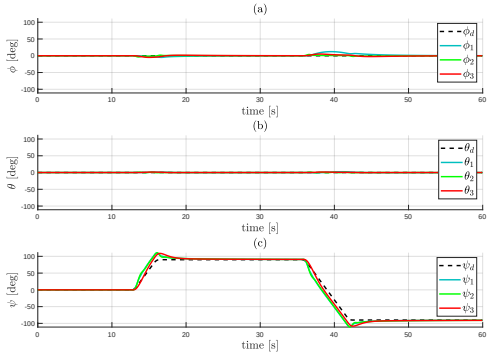

Figure 11: Comparison of the attitude of the vehicle using the three control methods. Blue line: LOS controller, Green line: SMC, Red line: Kinematic guidance principle using the $\mathcal{H}_r$ matrix. Top: Roll, Middle: Pitch, Bottom: Yaw

and moments. It notably creates two solutions for the widespread problem of tracking horizontal rails at constant depth lacking one actuated translations. The controller relies on a new matrix, $\mathcal{H}$, which allows controlling one translation of a virtual tracking point with one rotation. The algorithm calculating $\mathcal{H}$ is provided as well as design rules for using the method. The model-based cascade structure of the controller ensures good performance (GES) and natural robustness to external disturbances. The controller is shown to be as efficient as two well-known methods in the literature and provides a new solution, more practical than other methods, using roll instead of yaw for compensation and therefore allowing additional accurate yaw tracking.

One drawback of the method is that the behavior of the compensating degree of freedom is hardly predictable. Depending on the sway error to cancel, when using roll for instance, the vehicle can roll over and end up upside down, which can be damaging for some system or jeopardize some applications. Some further works will study the possible strategies to limit the damaging behavior of the compensating DOF.

Further works will also be needed to determine the optimal position of the tracking point E for a

given application, as well as other applications for this method. Furthermore, the method proposed in this work can easily be generalized and can offer several solutions for one problem as in this example. In some applications, one could imagine switching, during the mission, between the different solutions to modify the behavior of the vehicle locally and notably its attitude. This guidance principle could be straightforwardly associated with different control laws to enhance its robustness to external disturbances or model approximations.

Acknowledgments

The work of Loïck Degorre war supported by "*Région Bretagne*" (Grant 0311/ COH20007/ 00019559) and "*Brest Métropole*". This work was also supported by ISblue project, Interdisciplinary graduate school for the blue planet (ANR-17-EURE-0015) and co-funded by a grant from the French government under the program "*Investissements d'Avenir*".

References

Alonge, F., D'Ippolito, F., Raimondi, F.M., 2001. Trajectory tracking of underactuated underwater vehicles, in: 40th IEEE Conference on Decision and Control (CDC), Orlando, FL. pp. 4421–4426.

Antonelli, G., 2018. Underwater Robots. Number 123 in Springer Tracts in Advanced Robotics. 4th ed., Springer International Publishing, Cham.

Ashrafiuon, H., Muske, K.R., 2008. Sliding mode tracking control of surface vessels, in: IEEE American Control Conference (ACC), Seattle, WA. pp. 556–561.

Berge, S.P., Ohtsu, K., Fossen, T.I., 1999. Nonlinear control of ships minimizing the position tracking errors. Modeling, Identification and Control 20, 177–187. doi:10.4173/mic.1999.3.3.

Bishop, L.R., 1975. There is more than one way to frame a curve. Amer. Math. Monthly 82, 246–251.

Borhaug, E., Pavlov, A., Pettersen, K.Y., 2008. Integral LOS control for path following of underactuated marine surface vessels in the presence of constant ocean currents, in: 47th IEEE Conference on Decision and Control (CDC), Cancun, Mexico. pp. 4984–4991.

Breivik, M., Fossen, T.I., 2005. Principles of guidance-based path following in 2D and 3D, in: IEEE Conference on Decision and Control (CDC), Seville, Spain. pp. 627–634.

Caharija, W., Pettersen, K.Y., Bibuli, M., Calado, P., Zereik, E., Braga, J., Gravdahl, J.T., Sørensen, A.J., Milovanović, M., Bruzzone, G., 2016. Integral line-of-sight guidance and control of underactuated marine vehicles: Theory, simulations, and experiments. IEEE Trans. on Control Systems Technology 24, 1623–1642. doi:10.1109/TCST.2015.2504838.

Calvo, O., Rozenfeld, A., Souza, A., Valenciaga, F., Puleston, P.F., Acosta, G., 2008. Experimental results on smooth path tracking with application to pipe surveying on inexpensive AUV, in: Proc. IEEE/RSJ International Conference on Intelligent Robots and Systems (IROS), Nice, France. pp. 3646–3653.

Chen, H., Li, J., Gao, N., Han, J., Aït-Ahmed, N., Benbouzid, M., 2023. Adaptive backstepping fast terminal sliding mode control of dynamic positioning ships with uncertainty and unknown disturbances. Ocean Engineering 281, 114925. doi:https://doi.org/10.1016/j.oceaneng.2023.114925.

Chocron, O., Delaleau, E., 2019a. Task-based design of AUVs propulsion systems including fixed or vector thrusters, in: 45th Annual Conference of the IEEE Industrial Electronics Society (IECON), pp. 5292–5298.

Chocron, O., Delaleau, E., 2019b. Trajectory-based synthesis of propulsion systems for fixed-thrusters AUVs, in: Arakelian, V., Wenger, P. (Eds.), ROMANSY 22 — Robot Design, Dynamics and Control (Proceedings of the 22nd CISM IFToMM

Symposium, June 25–28, 2018, Rennes, France. Springer International Publishing, Cham, Switzerland. volume 584 of *CISM International Centre for Mechanical Sciences*, pp. 380–391.

Chocron, O., Vega, E.P., Benbouzid, M., 2018. Dynamic reconfiguration of autonomous underwater vehicles propulsion system using genetic optimization. Ocean Engineering 156, 564–579.

Degorre, L., Delaleau, E., Chocron, O., 2023. A survey on model-based control and guidance principles for autonomous marine vehicles. Journal of Marine Science and Engineering 11. doi:https://doi.org/10.3390/jmse11020430.

Degorre, L., Fossen, T.I., Delaleau, E., Chocron, O., 2024. A virtual reference point kinematic guidance law for 3-d path-following of autonomous underwater vehicles. IEEE Access vol. 12, pp. 109822–109831. doi:10.1109/ACCESS.2024.3440659.

Elmokadem, T., Zribi, M., Youcef-Toumi, K., 2016. Trajectory tracking sliding mode control of underactuated AUVs. Nonlinear Dyn 84, 1079–1091.

Elmokadem, T., Zribi, M., Youcef-Toumi, K., 2019. Control for dynamic positioning and way-point tracking of underactuated autonomous underwater vehicles using sliding mode control. Journal of Intelligent & Robotic Systems 95, 1113–1132. doi:10.1007/s10846-018-0830-8.

Encarnacao, P., Pascoal, A., 2000. 3D path following for autonomous underwater vehicle, in: Proceedings of the 39th IEEE Conference on Decision and Control (CDC), Sydney, NSW, Australia. pp. 2977–2982. doi:10.1109/CDC.2000.914272.

Fjellstad, O.E., Fossen, T.I., 1994. Position and attitude tracking of AUV's: a quaternion feedback approach. IEEE Journal of Oceanic Engineering 19, 512–518.

Fossen, T.I., 2021. Handbook of marine craft hydrodynamics and motion control. Second ed., Wiley, Hoboken, NJ & Chichester, West Sussex, UK.

Fossen, T.I., Aguiar, A.P., 2024. A uniform semiglobal exponential stable adaptive line-of-sight (ALOS) guidance law for 3-D path following. Automatica 163. doi:10.1016/j.automatica.2024.111556.

Fossen, T.I., Johansen, T.A., 2006. A survey of control allocation methods for ships and underwater vehicles, in: 14th Mediterranean Conference on Control and Automation, Ancona, Italy. pp. 1–6.

Gartner, N., Richier, M., Dune, C., Hugel, V., 2022. Hydrodynamic parameters estimation using varying forces and numerical integration fitting method. IEEE Robot. Autom. Lett. 7, 11713–11719.

Hung, N., Rego, F., Quintas, J., Cruz, J., Jacinto, M., Souto, D., Potes, A., Sebastiao, L., Pascoal, A., 2022. A review of path following control strategies for autonomous robotic vehicles: Theory, simulations, and experiments. Journal of Field Robotics 40, 747–779.

Isidori, A., 1989. Nonlinear Control Systems: An Introduction. 2nd ed., Springer-Verlag, Berlin.

Kelemen, M., 1986. A stability property. IEEE Trans. Automatic Control 31, 766–768.

Khalil, H.K., 2002. Nonlinear systems. 3rd ed ed., Prentice Hall, Upper Saddle River, N.J.

Korotkin, A.I., 2009. Added masses of three-dimensional bodies in infinite fluid, in: Added Masses of Ship Structures. Springer Netherlands, Dordrecht. volume 88, pp. 81–102. doi:10.1007/978-1-4020-9432-3_3.

Lamb, H., 2005. Hydrodynamics. 6th ed., Dover, New York. (Unabridged and unaltered republication of the 1932 ed., Cambridge University Press).

Lapierre, L., Soetanto, D., 2007. Nonlinear path-following control of an AUV. Ocean Engineering 34, 1734–1744. doi:10.1016/j.oceaneng.2006.10.019.

Lapierre, L., Soetanto, D., Pascoal, A., 2003. Nonlinear path following with applications to the control of autonomous underwater vehicles, in: 42nd IEEE International Conference on Decision and Control, IEEE, Maui, Hawaii, USA. pp. 1256–1261. doi:10.1109/CDC.2003.1272781.

Lawrence, D.G., Rugh, W.J., 1990. On a stability theorem for nonlinear systems with slowly varying inputs. IEEE Trans. Automatic Control 35, 860–864.

Lévine, J., Rouchon, P., 1994. An invariant manifold approach for robust control design and applications, in: Helmke, U., Mennicken, R., Saurer, J. (Eds.), Systems and Networks: Mathematical Theory and Applications (MTNS'93, Volume II, Invited and Contributed Papers), Akademie Verlag, Berlin. pp. 309–312.

Martin, S.C., Whitcomb, L.L., 2018. Nonlinear model-based tracking control of underwater vehicles with three degree-of-freedom fully coupled dynamical plant models: Theory and experimental evaluation. IEEE Trans. on Control Systems Technology 26, 404–414.

Micaelli, A., Samson, C., 1993. Trajectory tracking for unicycle-type and two-steering-wheels mobile robots. Technical Report 2097. INRIA. Sophia-Antipolis, France. 36 pages.

Nijmeijer, H., van der Schaft, A.J., 1990. Nonlinear Dynamical Control Systems. Springer-Verlag, New York.

Penrose, R., 1955. A generalized inverse for matrices. Mathematical Proceedings of the Cambridge Philosophical Society 51, 406–413. doi:10.1017/S0305004100030401.

Samson, C., 1993. Time-varying feedback stabilization of car-like wheeled mobile robots. The International Journal of Robotics Research 12, 55–64.

Shtessel, Y., Moreno, J.A., Plestan, F., Fridman, L.M., Poznyak, A.S., 2010. Super-twisting adaptive sliding mode control: A lyapunov design, in: Proc. 49th IEEE Conference on Decision and Control, Atlanta, GA, USA. pp. 5109–5113.

Vega, E.P., Chocron, O., Ferreira, J.V., Benbouzid, M., Meirelles, P.S., 2015. Evaluation of AUV fixed and vectorial propulsion systems with dynamic simulation and non-linear control, in: 41st Annual Conference of the IEEE Industrial Electronics Society (IECON2015), Yokohama, Japan. pp. 944–949.

Yoerger, D., Slotine, J.J.E., 1985. Robust trajectory control of underwater vehicles. IEEE Journal of Oceanic Engineering 10, 462–470.

Appendix A. Proof of Theorem 1

The stability of the control loop is proven for the seabed scanning task using the second compensation solution $\mathcal{H}_r$. The vehicle is considered sufficiently stable in roll and pitch to ensure $\phi = 0$ and $\theta = 0$ during operation because of the buoyancy of the vehicle and the relative positions of the centers of gravity and buoyancy[5]. Note that, when using the second compensation strategy $\mathcal{H}_p$, the roll angle of the vehicle is actively disturbed by the controller but its natural stability ensures that it converges back to zero when sway has converged. In this context, using (12) and (21), the closed-loop system can be expressed as[6]:

$$\begin{aligned} T\mathcal{H}_r T^{-1}(\dot{J}(\dot{\eta},\eta)^{-1}\dot{\eta}_d + J(\eta)^{-1}\ddot{\eta}_d) \\ + K(T\mathcal{H}_r T^{-1}\dot{J}(\dot{\eta},\eta)^{-1}\dot{\eta}_d - J(\eta)^{-1}\dot{\eta}_E) \\ = \dot{J}(\dot{\eta},\eta)^{-1}\dot{\eta}_E + J(\eta)^{-1}\ddot{\eta}_E \end{aligned} \quad \text{(A.1)}$$

Using (15) and after some calculations and trigonometric combinations, the two first lines of (A.1) lead

[5] If this is not the case, stability of the control loop can be established using more elaborated tools like Kelemen's Theorem (Kelemen, 1986; Lawrence and Rugh, 1990).

[6] Pleas note that $\dot{J}$ stands for the time-derivative of the matrix J.

to:

$$\ddot{e}_x + (K_p + K)\dot{e}_x + (K_i + KK_p)e_x + KK_i\chi_x + r(\dot{e}_y + K_p e_y + K_i\chi_y) = 0 \quad \text{(A.2a)}$$

$$\ddot{e}_y + (K_p + K)\dot{e}_y + (K_i + KK_p)e_y + KK_i\chi_y - r(\dot{e}_x + K_p e_x + K_i\chi_x) = 0 \quad \text{(A.2b)}$$

where $e_x = x_d - x_E$ and $e_y = y_d - y_E$ are the position errors of the tracking point along axes x_0 and y_0 of the inertial frame respectively, and $\dot{\chi}_x = e_x$, and $\dot{\chi}_y = e_y$ are their respective integrals. The stability of the controller is shown using a Lyapunov function and an simple argument stemming from linear systems theory. To do so, the following intermediate variable are introduced:

$$\sigma_x = \dot{e}_x + K_p e_x + K_i\chi_x \quad \text{(A.3a)}$$

$$\sigma_y = \dot{e}_y + K_p e_y + K_i\chi_y \quad \text{(A.3b)}$$

Note that (A.3a) can be understood as a linear input-output system with input σ_x, output e_x, and transfer function:

$$H(s) = \frac{s}{s^2 + K_p s + K_i} \quad \text{(A.4)}$$

It is always possible to guaranty that the poles of this transfer function have strictly negatives real parts with an appropriate choice of the gains K_p and K_i. The same remarks applies to (A.3b) with σ_y and e_y. The time evolution of the quantities σ_x and σ_y are respectively described by the dynamical system:

$$\dot{\sigma}_x = -K\sigma_x - r\sigma_y \quad \text{(A.5a)}$$

$$\dot{\sigma}_y = -K\sigma_y + r\sigma_x \quad \text{(A.5b)}$$

Note that the complete dynamical system (A.3)–(A.5) let naturally appear a cascade structure. Consider the Lyapunov function candidate for the equilibrium point $(\sigma_x, \sigma_y) = (0, 0)$ of (A.5a)–(A.5b):

$$V = \frac{1}{2}(\sigma_x^2 + \sigma_y^2) \quad \text{(A.6)}$$

This function is $\mathcal{C}^1$, strictly positive definite and radially unbounded; its first order time derivative reads:

$$\begin{aligned}\dot{V} &= \dot{\sigma}_x\sigma_x + \dot{\sigma}_y\sigma_y \\ &= -K\sigma_x^2 - \dot{\psi}\sigma_x\sigma_y - K\sigma_y^2 + \dot{\psi}\sigma_x\sigma_y \\ &= -K(\sigma_x^2 + \sigma_y^2) \end{aligned} \quad \text{(A.7)}$$

is thus, for any strictly positive gain K, strictly negative definite and, moreover, $\dot{V} \leqslant -\alpha V$ with $\alpha \geqslant 2K$. Consequently, the equilibrium point $(\sigma_x, \sigma_y) = (0, 0)$ is globally exponentially stable (GES)[7]. Finally, as the transfer function (A.4) is stable, convergence of σ_x and σ_y to 0 implies convergence of e_x and e_y to 0. □

[7] Note that in (Khalil, 2002, Lemmas 9.2 and 9.3) shows that exponential stability provides robustness to small uniformly bounded disturbances.